Second-order silicon photonic differential-equation solver for general linear time-invariant systems

Junming Mao, Jiayang Wu, Ting Pan, Boyu Liu, Jizong Peng, Huanying Zhou, Ciyuan Qiu, and Yikai Su

State Key Laboratory of Advanced Optical Communication Systems and Networks, Department of Electronic Engineering, Shanghai Jiao Tong University, Shanghai 200240, China, E-mail: yikaisu@sjtu.edu.cn

Abstract — **We propose and experimentally demonstrate an on-chip silicon photonic differential-equation solver that can be used to solve second-order constant-coefficient ordinary-differential-equations (ODEs). The feasibility of the device is verified by 5 and 10 Gb/s optical signals.**

Keywords — **all–optical information processing, second-order differentiator, silicon photonics.**

I. INTRODUCTION

Differential equations model and govern fundamental phenomena and applied processes in almost any field of science and engineering [1]. As fundamental differential equations, constant-coefficient linear ordinary differential equations (ODEs) are widely employed in characterizing linear time-invariant (LTI) systems [2]. All-optical ODE solvers could potentially offer processing bandwidths that are orders of magnitude larger than their electronic counterparts [3], thus possessing advantages in high-speed computing and information processing. In our previous reports, first-order photonic ODE solvers characterizing LTI systems were demonstrated [4, 5]. On the other hand, high-order ODE solvers are also of great significance and widely employed in optical pulse shaping and analog signal processing [6].

In this paper, we propose and experimentally demonstrate a second-order silicon photonic differential-equation solver for general LTI systems. The proposed device is monolithically integrated on a silicon-on-insulator (SOI) wafer with a compact footprint of 70 μm × 50 μm. Second-order ODE solving experiments at data rates of 5 and 10 Gb/s are carried out for three typical input pulse waveforms, i.e., sinusoidal-like, super-Gaussian-like, and Gaussian-like pulse trains. The experimental results show good agreement with numerical solutions of the ODEs and verify the effectiveness of the proposed devices as an on-chip second-order ODE solver.

II. OPERATION PRINCIPLE AND DEVICE FABRICATION

Figure 1(a) illustrates the schematic configuration of our proposed second-ODE solver. The system block diagram is shown in Fig. 1(b). The red path and the blue path indicate the feedback branch and the forward trunk, respectively. The block in the center denotes the microring resonators (MRRs) as linear first-order optical filters. The scalar multipliers with various factors represent the constant coefficients multiplied to the amplitude of the complex optical field. r_i and κ_i ($i = 1, 2$) are the transmission and cross-coupling coefficients of the two directional coupler, respectively. T_1, T_2, and T_3 are the transmission factors along the three parts of the feedback loop between the MRR and the two directional couplers. The block with a factor of j is introduced by Coupler 1 or 2, which can be combined into the phase shift along the input or output channel
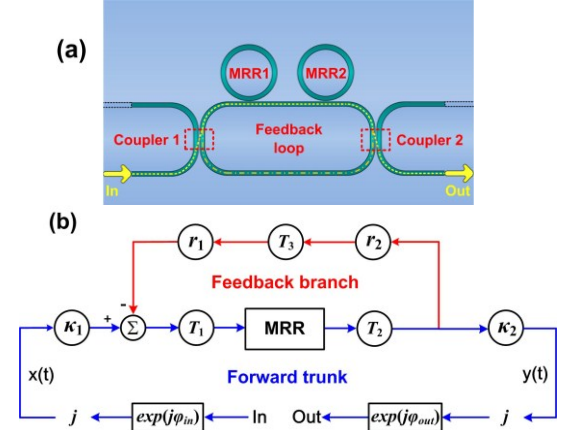
Fig. 1. (a) Schematic configuration of the proposed ODE solver. (b) System block diagram of the ODE solver in (a).

shown by the block with a factor of exp ($j\varphi_{in}$). Feedback subtraction can be realized when the phase shift along the feedback loop is $(2N+1)\pi$ ($N=0, 1, 2\ldots$). After processed by the ODE solver in Fig. 1(a), the complex optical field of the output signal y(t) can be related to that of the input signal x(t) based on the system block diagram in Fig. 1(b) as [5]:

$$\frac{d^2y(t)}{dt^2} + a_1\frac{dy(t)}{dt} + a_0y(t) = \frac{d^2x(t)}{dt^2} + b_1\frac{dx(t)}{dt} + b_0x(t) \tag{1}$$

where

$$a_1 = \frac{(\alpha_1+\alpha_2)+T_{feedback}(\beta_1+\beta_2)}{1+T_{feedback}}, a_0 = \frac{\alpha_1\alpha_2 + T_{feedback}\beta_1\beta_2}{1+T_{feedback}}$$

$$b_1 = \beta_1+\beta_2, b_0 = \beta_1\beta_2.$$

In Eq. (1), $T_{feedback} = r_1r_2T_1T_2T_3$ and $T_{forward} = \kappa_1\kappa_2T_1T_2$ are the overall transmission factors along the feedback loop and the forward trunk, respectively. $\alpha_{1,2} = \omega_0/2Q_{i1,2} + \omega_0/2Q_{e1,2}$ and $\beta_{1,2} = \omega_0/2Q_{i1,2} - \omega_0/2Q_{e1,2}$ are the constant coefficients, with ω_0, $Q_{i1,2}$, and $Q_{e1,2}$ denoting the carrier frequency of input optical signal, the quality factors induced by internal cavity loss, and the quality factors induced by external coupling, respectively. Compared to the formula in [6], the ODE in Eq. (1) includes additional first- and second-order derivative terms of input signal, allowing for a more general and versatile modeling of LTI systems. The constant coefficient of $d^2x(t)/dt^2$ is normalized to 1. Given that there are other amplifications or attenuations in practical processing process, the difference in amplitude can be further compensated. For high-speed optical signals on the order of Gb/s, the differential item dt is in units of picosecond. The constant coefficients a_0, b_0, a_1, and b_1 can be set accordingly to process high-speed optical signal.

The designed device was fabricated on an 8-inch SOI wafer. The micrograph of the device is shown in Fig. 2(a). 248-nm
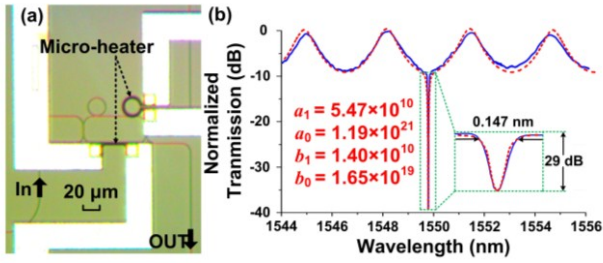
Fig. 2. (a) Micrograph of the fabricated second-order ODE solver. (b) Measured transmission spectrum of the device in (a).

deep-ultraviolet (DUV) photolithography was utilized to define the device layout, and an inductively coupled plasma (ICP) etching process was used to etch top silicon layer. Grating couplers for TE polarization were employed at the ends of the input and output ports. Thermal-optic micro-heaters are fabricated to control the phase shift for feedback subtraction. The cross sections of the single-mode silicon waveguides are 450 nm $\times$ 220 nm, and the gap size in the straight coupling regions is ~180 nm. The radii of the two MRRs are ~10 μm, and the circumference of the feedback loop is ~186 μm. The straight coupling length of Coupler 1 and 2 is ~11.5 μm, thus 3-dB coupling ($r_i \approx \kappa_i$, $i = 1, 2$) around 1550 nm can be achieved. The measured transmission spectrum of the fabricated device is shown in Fig. 2(b) by the blue solid curve. The fitted curve obtained by using the scattering matrix method is also shown by the red dashed curve accordingly. The fitting parameters are Q_{i1} = Q_{i2} = ~3.05 $\times$ 10^4, Q_{e1} = Q_{e2} = ~2.73 $\times$ 10^4, and $T_{feedback}$ = ~0.5006. The calculated constant coefficients in Eq. (1) are also shown in Fig. 2(b). There are two types of resonances in the transmission spectrum: the resonance notches induced by the MRRs, and the resonance peaks caused by the feedback loop. Due to weak external coupling and short circumferences, the resonance notches of the MRRs exhibit high quality factors and small free spectral ranges (FSRs) relative to the resonance peaks of the feedback loop. In Fig. 2(b), the resonance notches of the two MRRs coincide with the valley between adjacent resonance peaks of the feedback loop at 1549.758 nm, where the phase shift along the feedback loop is $(2N+1)\pi$ (N=0, 1, 2…).

III. SECOND-ORDER ODE SOLVING EXPERIMENT

We use the experimental setup shown in Fig. 3 to test the
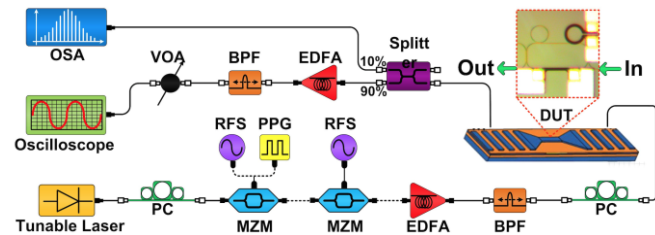
Fig. 3. Experimental setup of second-order ODE solving experiment. PC: polarization controller. MZM: Mach-Zehnder modulator. RFS: radio frequency synthesizer. PPG: pulse pattern generator. EDFA: erbium-doped fiber amplifier. BPF: band pass filter. DUT: device under test. VOA: variable optical attenuator. OSA: optical spectrum analyzer.

performance of the fabricated device. Three types of input pulse waveforms are generated in our experiments [7]: (I) sinusoidal like, (II) super-Gaussian-like, and (III) Gaussian-like pulse train.
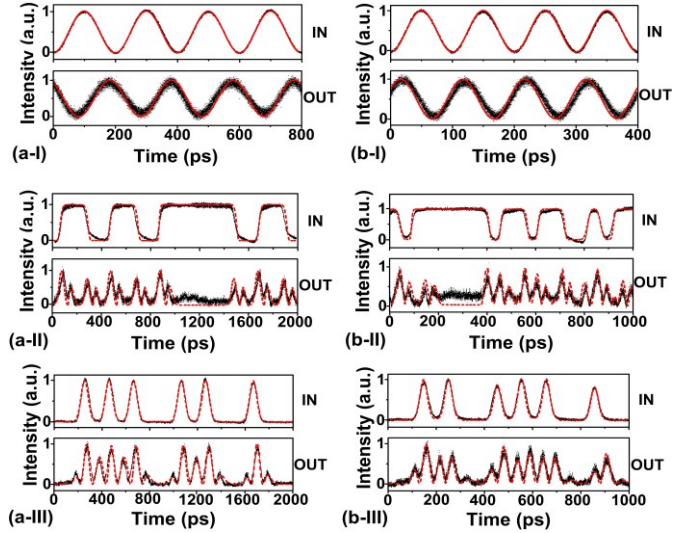
Fig. 4. (a-I)–(a-III) Three types of input optical pulse waveforms at data rate of 5 Gb/s and the corresponding output pulse waveforms after processed by the second-order ODE solver. (b-I)–(b-III)Three types of input optical pulse waveforms at data rate of 10 Gb/s and the corresponding output pulse waveforms after processed by the second-order ODE solver.

Two data rates of 5 and 10 Gb/s are chosen for each type. The experimentally results are shown in Fig. 4 by the black solid curves. The fitted $x(t)$ and numerically calculated $y(t)$ in Eq. (1) with coefficients equaling to the calculated values in Fig. 2(b) are represented by the red dashed curves accordingly. The amplitudes are normalized for clear observation. It can be seen that the observed output waveforms closely approximate the numerical solution for all the three types of input waveforms. The agreement verifies the feasibility of the proposed device as a second-order ODE solver.

IV. CONCLUSION

In conclusion, we have proposed and experimentally demonstrated a second-order silicon photonic ODE solver. System demonstration has been performed at data rates of 5 and 10 Gb/s with three signals including sinusoidal-like, super-Gaussian-like, and Gaussian-like pulse trains. The experimental results verify the effectiveness of the proposed device as an on-chip second-order ODE solver.

V. ACKNOWLEDGEMENT

REFERENCES

[1] G. F. Simmons, *Differential equations with applications and historical notes* (McGraw-Hill, 1991), Chap. 1.
[2] A. V. Oppenheim, *et al.*, *Signals and Systems* (Prentice-Hall, 1996), Chap. 2.
[3] K. Y. Yun, *et al.*, "The design and verification of a high-performance low-control-overhead asynchronous differential equation solver," IEEE Trans. VLSI Syst. **6**, 643−655 (1998).
[4] L. Lu, *et al.*, "Compact all-optical differential-equation solver based on silicon microring resonator," Frontiers of Optoelectronics 5, 99–106 (2012).
[5] J. Wu, *et al.*, "Compact tunable silicon-photonic differential-equation solver for general linear time-invariant systems," Opt. Express, **22**(21): 26254–26264 (2014).
[6] S. Tan, *et al.*, "High-order all-optical differential equation solver based on microring resonators," Opt. Lett. **38**(19), 3735−3738 (2013).
[7] P. J. Winzer and R. J. Essiambre, "Advanced optical modulation formats," Proc. IEEE **94**, 952−985 (2006).